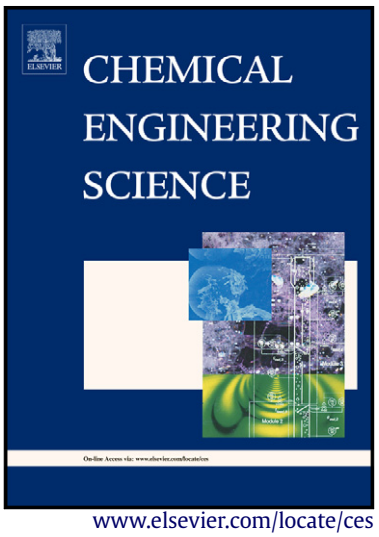

Size control of carbon-supported platinum nanoparticles made using polyol method for low temperature fuel cells

P.C. Favilla, J.J. Acosta, C.E. Schvezov, D.J. Sercovich, J.R. Collet-Lacoste

www.elsevier.com/locate/ces

PII: S0009-2509(13)00408-9
DOI: http://dx.doi.org/10.1016/j.ces.2013.05.067
Reference: CES11112

To appear in: *Chemical Engineering Science*

Received date: 16 November 2012
Revised date: 31 May 2013
Accepted date: 31 May 2013

Cite this article as: P.C. Favilla, J.J. Acosta, C.E. Schvezov, D.J. Sercovich, J.R. Collet-Lacoste, Size control of carbon-supported platinum nanoparticles made using polyol method for low temperature fuel cells, *Chemical Engineering Science,* http://dx.doi.org/10.1016/j.ces.2013.05.067

SIZE CONTROL OF CARBON-SUPPORTED PLATINUM NANOPARTICLES MADE USING POLYOL METHOD FOR LOW TEMPERATURE FUEL CELLS

P.C. Favilla [a,c,*], J.J. Acosta [a,c], C.E. Schvezov [a], D.J. Sercovich [b], J.R. Collet-Lacoste [c]

a) FCEQyN, UNaM, Felix de Azara 1552, (N3300LQN), Posadas, Misiones. Argentina

b) H2-TEC. Tte. B. Matienzo 1799, (C1426DAE), CABA. Argentina

c) U. A. Materiales, CNEA, Av. Gral. Paz 1499, (B1650KNA), San Martín, Buenos Aires. Argentina

Abstract

The aim of this work is to present the results of the synthesis of Pt nanoparticles using the modified polyol method, using carbon black powder Vulcan XC-72R as a support. Two different techniques were used to synthesize the catalysts: a) fixing the initial concentration of the precursor (2 mM in H_2PtCl_6) while adding the required amount of support to obtain different nominal loads of platinum; b) changing the initial concentration of the precursor to obtain altogether 10 *wt.%* nominal load of platinum. Catalysts were characterized using X-ray diffraction, transmission electron microscopy and cyclic voltammetry. The particles obtained ranged in sizes between 2.2 and 6.2 nm. These sizes were controlled by the initial concentration of the precursor. It has been found that the concentration of nanoparticles formed during synthesis was the same regardless of a) the initial concentration of the precursor and b) the amount of carbon support. In order to explain experimental results a new and simple statistical and geometrical treatment is used.

Keywords: Catalyst support; Particle formation; Electrochemistry; Nanostructure; Fuel cell; Electrocatalyst

* Corresponding author. Phone: +54 11 6772 7271; fax: +54 11 6772 7362; e-mail: favilla@cnea.gov.ar

List of abbreviations and symbols

CV: Cyclic voltammetry.

ECSA : Electrochemical surface area.

PVP: Polyvinylpyrrolidone.

TEM: Transmission electron microscopy.

RHE: Reversible hydrogen electrode.

XRD: X-ray diffraction.

A^T : Total area.

$\overline{A}$: Geometrical specific area.

C : Specific charge of a monolayer of adsorbed hydrogen atoms (typically 210 μC cm^{-2}).

c_P^i : Initial concentration of the precursor.

$\overline{d}$: General mean diameter of nanoparticles.

$\overline{d}_{\mathrm{XRD}}$: Crystallite diameter of nanoparticles defined as the cubic root of the crystallite volume.

$\overline{d}_{TEM}$: Mean diameter of nanoparticles calculated by TEM.

k : Scherrer's constant.

m_{Pt} : Mass load of platinum on the electrode.

m_T : Total metal mass in a synthesis.

m_S : Total mass of substrate (carbon).

MW : Molecular weight.

$N_{np}(r)$: Number of nanoparticles with radius r.

N_{np}^T : Total number of nanoparticles in a synthesis.

Q: Area of the desorption peaks of hydrogen.

$\bar{r}$: Mean radius of nanoparticles in the distributions.

v_S : Voltage scan rate.

V^T : Total volume.

V_m : Volume of nanoparticles with mean diameter $\bar{d}$.

V_r : Volume of reaction.

wt %: percent mass fraction of metal in catalyst.

Greek symbols

α: Relative standard deviation in radius or diameters.

β : Full width at half maximum (FWHM) in radians.

σ_r : Standard deviation of the radius distribution.

σ_d : Standard deviation of the diameter distribution.

λ : Wavelength Co Kα.

θ : Bragg peak angle.

ρ_M : Metal density.

ρ_{np} : Density of nanoparticles per unit reaction volume. ($\rho_{np} = N_{np}^T / V_r$)

η_A : Area efficiency.

1. Introduction

Catalysts used in gas diffusion electrodes have become key materials in low temperature fuel cells. Catalysts based on platinum are used because of their high activity and stability (Adzic et al., 2007; Bagotsky, 2009; J Zhang et al., 2005; J. Zhao et al., 2011). Synthesis of dispersed Pt supported catalysts has been widely used in electrodes developed for fuel cells (H. Oh et al., 2007; Senthil Kumar et al., 2010; Vengatesan et al., 2008). Black carbon materials have been

used to improve electrical conductivity and dispersion of active material. Because of the requirements of electrical conductivity, the carbons used need to have a certain degree of graphitizing to lower its ohmic resistance. Fuel cell electrodes are to be economical and efficient, so the Pt load must be minimized while maximizing the specific area. Different ways are typically used to achieve a reduction in the metal load: one of them is the control of the size of the nanoparticles used (Kinoshita, 1990; Minhua Shao et al., 2011) and the other is the formation of alloys, either skin or core-shell structure, by combination with other metals (Yano et al., 2007; J. Zhao et al., 2011).

The limiting step in low temperature fuel cells is the oxygen reduction reaction (ORR), one of the most important reactions in electrochemistry. ORR seems to depend on the size of the Pt nanoparticles (Bagotsky, 2009; Leontyev et al., 2011) but this is under debate (Nesselberger et al., 2011). Nevertheless, monodispersions of nanoparticles is required when we wish to study the effects of their diameters on the physical properties of catalysts.

Among the many methods of synthesis of catalysts (Bock et al., 2004; Liu et al., 2006; H.-S. Oh et al., 2008; Yano et al., 2007), the method most widely used to generate colloidal suspensions of metals is the reduction of transition-metal salts in solution. In fact, this method is quite simple to implement. A wide range of reducing agents have been used to obtain colloidal materials: gases such as hydrogen or carbon monoxide, hydrides or salts such as sodium boron hydride or sodium citrate, or even oxidative solvents such as alcohols. The different reduction methods of the Pt precursors, which differ in the reduction agent used, are described in literature. These include the formic acid method (Liu et al., 2006; Prabhuram et al., 2003, 2004; W. Zhou et al., 2003), impregnation method followed by reduction with hydrogen at high temperature (Liu et al., 2006) and microwave-assisted polyol (Chu et al., 2010) or polyol method (Chen and Xing, 2005).

In a series of papers Finke and co-workers, (Watzky and Finke, 1997; Besson et al. 2005, Watzky et al., 2008) present the first examples of nanoparticles that are suitable for in-depth mechanistic studies and show a way of monitoring the formation of nanoparticles in real time According to these authors, the acting mechanism consists in four steps (double autocatalytic step mechanism):

$$nP^{+X} + (red.) \xrightarrow{k_1} P_n^0 \qquad \text{slow continuous nucleation (i)}$$

$$P_n^0 + P^{+X} + (red.) \xrightarrow{k_2} P_{n+1}^0 \qquad \text{autocatalytic surface growth (ii)}$$

$$P_n^0 + P_m^0 \xrightarrow{k_3} P_{n+m}^0 \qquad \text{agglomeration step (iii)}$$

$$P_n^0 + P_{Bulk}^0 \xrightarrow{k_4} P_{Bulk}^0 \qquad \text{autocatalytic agglomeration (iv)}$$

As Finke et al. claim, one of the conditions for synthesis of "near" mono-dispersed nanoparticles is the separation in time of the nucleation and growth steps If all nuclei are initially formed with similar sizes and are uniformly distributed, they will statistically grow at the same rate since they are indistinguishable and surrounded by the same chemical environment. The term "near" is applied considering that the thermal fluctuations in the concentration of the precursor define the final diameter distribution. In this sense, materials that are "near" mono-dispersed are the ones that present higher specific areas: the ratio area/volume is inversely proportional to the diameter.

The formation mechanism of nanoparticles in this process is complex since it takes place in a heterogeneous phase and depends on both; the rate of reaction and the transport properties. The latter can vary with the degree of completion of the reaction. In addition, when a clear separation between nucleation and growth steps is not achieved, the grown particles may present a large diameter- dispersion and a low specific area.

In order to avoid agglomeration of nanoparticles (reactions iii and iv), protective agents of steric or electrostatic nature are used. Macromolecules such as polymers or oligomers are used

to stabilize the colloid, (i.e. PVP in the case of polyol methods). The resulting adsorption of macromolecules onto the surfaces of the nanoparticles provides a protective layer against agglomeration by restricting the motion of the colloid in the space between the particles. This causes both a decrease in entropy and an increase in free energy (Roucoux et al., 2002). Nevertheless, the addition of macromolecules also influences the rates of reaction for nucleation and growth, e.g. viscosity of the environment is changed, and the diffusion coefficients of the involved species also change.

Electrostatic stabilization can be achieved using ionic solutions of compounds such as halides, polyoxoanions or carboxylates (Watzky and Finke, 1997; Watzky et al., 2008). The adsorption of these compounds and their related counter-ions onto the metallic surface create an electric double-layer around the particles generating electrostatic repulsion between them.

In the present paper the results obtained on the synthesis of Pt nanoparticles by the modified polyol method are discussed. The characterization of the catalysts is carried out by correlating the XRD, TEM and CV measurements. The results show that the nanoparticle diameters were near-monodisperse with a Gaussian distribution. Their sizes were controlled by the initial concentration of the precursor, regardless of the Pt loading within certain limits. One of the conclusions of this work is that in the case of the synthesis of Pt nanoparticles through the polyol method, the concentration of nanoparticles in the solution after synthesis was constant independently of the initial concentration of the precursor. A new and simple statistical and geometrical treatment is presented in Appendix "A" which is used to explain the experimental results.

2. Experimental

2.1 Pt/C synthesis

The nanoparticles of Pt were prepared using the modified polyol method (Chen and Xing, 2005). The solvent and reducing agent was an ethylene glycol/water (volume ratio 3:1)

solution. The catalysts were prepared with a protecting agent PVP to prevent the subsequent agglomeration of nanoparticles (reactions iii and iv). The support material in all cases was carbon black powder (Vulcan XC-72R, Cabot international) with area BET 250 $m^2\ g^{-1}$. The platinum precursor was H_2PtCl_6.

The typical catalyst preparation involves dissolving the precursor in ethylene glycol/water solution and adding a predetermined amount of black carbon. The amount of precursor used was determined by the desired Pt mass loading in the catalyst, which is defined as the weight percentage of Pt in the catalyst consisting of Pt and carbon. The amount of PVP added to the solution was measured in relation to the mass of Pt using a molar ratio of PVP/Pt equal to 0.1 (referred to monomer unit of PVP). This proportion was calculated considering Chen and Xing's work (Chen and Xing, 2005) in which the authors demonstrate that the catalyst active surface area is high and can be maintained at a high level, even if the Pt loading reaches 35 *wt.*%.

Reduction of the precursor was achieved through heating at a 2ºC min^{-1} rate and keeping the polyol solution on reflux for an hour under continuous magnetic stirring. After the polyol solution was cooled-down to room temperature, the catalysts were filtered, washed with Milli-Q (Milipore) water 18.2 MΩ cm and dried in vacuum at 80ºC for 3 hs. The synthesis of final catalysts (Pt + carbon) was done by two different ways:

a) Taking c_P^i fixed at 2 mM and adding the required amount of support to obtain different Pt nominal loads, *wt.*%, defined as : $wt.\% = 100\, m_{Pt} / (m_{Pt} + m_S)$.

b) Changing the initial concentration of the precursor to obtain a total 10 *wt.*% nominal Pt load.

Measurements of *wt.*% were done in duplicates by gravimetric method, approx. 0.1 g of sample, previously washed in distilled water and dried in a ceramic melting pot, tared with an analytical scale (±0.01mg). Samples were dried in an oven with high purity N_2 at 100ºC, cooled down and weighed again using the same scale. Samples were then calcinated in the same oven

circulating clean air at 600ºC for 3 hours (enough time to guarantee the total oxidation of the Carbon). Cooling was done turning off the oven and passing a current of pure N_2 until room temperature was attained. The melting pot containing the metal Pt was once again weighed. The *wt.%* was calculated by difference.

2.2 Physical characterization

All samples were analized with an X-3000 Philips powder X-ray diffractometer using Co Kα radiation. The crystallite sizes were determined using peak (111) according to Scherrer's equation:

$$\bar{d}_{XRD} = \frac{k\,\lambda}{\beta \sin\theta} \tag{1}$$

The scans in θ covered the range between 10º-110º and were programmed to a nominal 0.033º step size with a 2 s time per step.

The characterization by transmission electron microscopy was performed on TEM Philips EM 301 operated at 60 kV. For each catalyst more than 300 nanoparticles were counted in order to determine the histograms of nanoparticle diameters, mean diameters and standard deviation, which were calculated as:

$$\bar{d} = \frac{1}{n}\sum_i^n d_i \tag{2}$$

$$\sigma_d = \left(\frac{1}{n-1}\sum_i^n (d_i - \bar{d})^2\right)^{1/2} \tag{3}$$

2.3 Electrochemical characterization

Electrochemical surface area was evaluated from hydrogen desorption by CV in a three-electrode electrochemical cell using a potentiostat/galvanostat, the working electrode was a gold disk with a 0.196 cm^2 area and the counter electrode and the reference electrode, a Pt wire and a reversible hydrogen electrode (RHE), respectively.

On the surface of the working electrode, 20 μL of catalyst ink were spread and dried in air for 600 s at 100ºC and then coated with 20 μL Nafion® 5 % and dried again at 100ºC for 600 s in air. The process of ink preparation was the following: 4 mg of catalyst were ultrasonically suspended in 2 mL of a water-isopropyl alcohol (volume ratio 1:1) solution for 600 s. Experiments were conducted in a N_2-saturated solution of 0.5 M H_2SO_4, thermostatic at 30ºC (±0.1ºC).

All electrodes were subject to cycling between -0.080 V and +1.230 V (RHE) with a scan rate of 0.040 V s^{-1}. Reproducibility of the results were verified by triplicate.

ECSA was calculated from the area Q of the hydrogen desorption peaks taking as a baseline the current of the double layer using the equation:

$$\mathrm{ECSA} = \frac{Q}{C\, v_S\, m_{Pt}} \tag{4}$$

Where m_{Pt} is the mass load of platinum on the golden electrode.

3. Results and discussion

3.1 Physical characterization

All catalyst samples observed by TEM showed a Gaussian and uniform narrow distribution of the nanoparticle diameters on the support (Fig. 1). The relative dispersion to their mean diameter, defined as $\alpha = \sigma_d / \overline{d}$, had similar values for all catalysts. When c_P^i was changed from 0.25 to 12 mM (48 times) the values of α were almost constant (a 50 % change), as shown in Tables I and II. A mean value of $\alpha = (0.26 \pm 0.04)$ was determined with the eleven data. The TEM observations showed that the nanoparticle size increased when the c_P^i value in the synthesis increased.

Figure 2 shows the diffractograms obtained on catalysts with different Pt loads and different "c_P^i."s. All diffractograms showed the characteristic peaks for Pt. Tables I and II display the calculated crystallite sizes using eq. (1).

Figure 3 shows a graph of the mean diameters evaluated by means of XRD and TEM. A very good correlation between crystallite sizes and mean diameters was observed. Values of crystallite sizes obtained by XRD were 20 % smaller than mean diameters obtained through TEM. In this work the value obtained by TEM was taken as the diameter value.

3.2 Importance of the initial concentration of the precursor

From the c_P^i and experimental results showed in Tables I and II it is possible to establish the following:

- For those syntheses performed at a 2 mM of H_2PtCl_6 fixed initial concentration of the precursor and varying the nominal load of Pt, ECSA values and nanoparticles diameter result practically identical (Table I),

- For those syntheses performed increasing the c_P^i, yet maintaining the nominal 10 % Pt load, an increase in the diameter was systematically observed together with a decrease in ECSA (Table II).

These results demonstrate that c_P^i is one of the most important factors in the control of the mean diameter of nanoparticles and therefore in the ECSA ; it does not depend on the Pt load in the support as claimed in the bibliography (Bergamaski et al., 2006; Geniès et al., 1998; Maillard, 2002; Nores-Pondal et al., 2009; Perez et al., 1998), at least between 10 and 40 % nominal loads. On the other hand, other factors in the control of the mean diameter of nanoparticles exist, such as the influence of PVP in the processes of nucleation and/or growth. In measurements performed with ratios of PVP/Pt of 0.1 and 1, the diameter increased only a 3 % (i.e. from 2.86 to 2.95 nm), whereas the ECSA diminished in a 15 % (i.e. from 66 to 58 $m^2 g^{-1}$). This is in accordance with (Chen and Xing, 2005) in their conclusion that high PVP concentrations did not result in large activate surface areas, and this was attributed to the blocking effects of the PVP polymers in the electrochemical measurements. The addition of

carbon before synthesis results in nanoparticles that are smaller than those obtained if carbon is added later on in the process (a 5 % smaller). This shows that the addition prior to the process of synthesis increases the number of nuclei, which are smaller in size, because the total load of Pt is the same.

3.2.1 Consideration and determination of the concentration of nanoparticles in solution

Taking into account eq. (A.11) in appendix A the mean volume of nanoparticles V_m is proportional to c_P^i and inversely proportional to ρ_{np}. Figure 4 shows an experimental proportionality between V_m and c_P^i, within experimental error (correlation factor of 0.986), for all the measurements performed in this work. This behavior shows that the value of ρ_{np} did not change independently of c_P^i. From this consideration, ρ_{np} was evaluated from the value of $Slope\ 1$ obtained from Fig. 4 and Eq. (A.11), using the following equation:

$$\rho_{np} = \frac{MW}{(1+3\alpha^2)\,\rho_M\ Slope\ 1} \tag{5}$$

The nanoparticle concentration ρ_{np} resulted to be $(6.0 \pm 2.6)10^{14}$ nanoparticles cm^{-3}. This constancy in ρ_{np} means that during the nucleation process the number of effective nuclei is controlled by a steric constraint within the volume of reaction, regardless of the value of c_P^i.

Walzky et al (see data reported on Table 1 in ref. Watzky et al.'s, (2008)) show very similar diameters (i.e. 2.1 nm) for nine different solutions in the synthesis of Ir nanoparticles using the same c_P^i. They show that within experimental error, the values of ρ_{np} were similar in the nine synthesis performed using different precursors but the same c_P^i (i.e. 1.2 mM). This result obtained in different synthesis media, supports the idea that the mechanism proposed by Watzky and Finke (1997), Besson et al. (2005) Watzky et al.'s, (2008) is a more general one which could be valid for the synthesis of nanoparticles of other transition metals. This is an interesting perspective to investigate in the future.

3.3 Electrochemical measurements

3.3.1 General results from CV

All voltammograms (Fig. 5a and 5b) show the characteristic peaks of hydrogen adsorption/desorption processes, the double-layer region (+0.400 to +0.650 V_{RHE}), oxidation and reduction of Pt. The strong and weak peaks of hydrogen adsorption/desorption were observed as well as two peaks for the oxidation of the surface Pt and a peak related to the reduction of the layer of surface oxide formed.

The smaller the size of the nanoparticles, the greater the shift of the peak of reduction of Pt oxide toward more negative potentials in the voltammogram. This phenomenon has been explained on the basis of the change in the adsorption energy on low coordination sites, which are very abundant with nanoparticles smaller than 2 nm (Minhua Shao et al., 2011).

Some authors (Chen and Xing, 2005; Pozio et al., 2002; Prabhuram et al., 2003, 2004) have calculated ECSA using the area of the hydrogen adsorption peaks, desorption peaks or a mean value of these. In our case, ECSA values were obtained from the hydrogen-desorption peak area and eq. (4) because desorption peaks resulted to be independent of the value of v_S. Values calculated using the adsorption peaks provide higher values of ECSA because of the extra current contribution of the discharge of gaseous hydrogen.

Figure 5a shows the voltammograms of catalysts synthesized with a fixed c_P^i. Voltammograms corresponding to catalysts synthesized in 2 mM show the same areas for the hydrogen desorption peaks. They therefore have the same ECSA, i.e. (64±1) $m^2\ g^{-1}$. A decrease in the c_P^i produces an increase in the area of hydrogen desorption (Fig. 5b); except for very low concentrations.

As can be seen in Fig. 6, there is a proportional relationship between ECSA and $c_P^{i\ -1/3}$ in the range between 0.5 and 4 mM. This behavior is predicted by Eq. (A.23). A value for η_A was

obtained from the expression of the slope. This value is the quotient between the experimental effective area for the hydrogen desorption peak and the geometrical area, which is equal to:

$$\eta_A = Slope2\,\frac{(1+3\alpha^2)^{2/3}}{(1+\alpha^2)}\left[\frac{MW\,\rho_M{}^2}{36\,\pi\,\rho_{np}}\right]^{1/3} \tag{6}$$

Taking the values of ρ_{np} and α previously evaluated, and the value for the *slope 2* calculated from Fig. 6, the value for $\eta_A = (0.77 \pm 0.12)$ was obtained (considering the TEM diameters as the accurate ones). Given that ρ_{np} is constant and independent of c_P^i, one could expect η_A to be independent as well. This factor η_A suggests that it is not possible to electrochemically use the 100 % of the geometrical surface (Chen and Xing, 2005; Esparbé et al., 2009; J. W. Kim et al., 2011; H. Oh et al., 2007). According to this factor, there is a (23±4) % decrease in the value of the geometrical area. Different reasons could explain this factor: agglomeration of nanoparticles, nanoparticles with no good electrical contact, errors when determining the baseline generated by the contribution of the support double layer, loss of active area in those parts of Pt in contact with the support among others.

Figure 6 shows that the experimental result for the value of ECSA at 0.25 mM (i.e. < 2.2 nm) is lower than the value extrapolated from proportional relation with $c_P^{i\,-1/3}$. The experimental values of ECSA for 8 and 12 mM are smaller than the values predicted by the fit. For these concentrations, agglomeration of nanoparticles was experimentally observed by TEM, as shown in Fig. 1a. On the other hand, mean diameters of nanoparticles measured by TEM correspond with the value predicted by Eq. (A.11). This means that the catalysts have the necessary specific geometrical area to give the extrapolated value of ECSA (Fig. 6), but their effective active surface is smaller as shown experimentally by the ECSA measure. This enables us to assign the experimental decrease in the value of ECSA mainly to agglomeration.

3.4. The influence of the distributions of diameters in the ECSA

One of the conditions for synthesis of near-monodisperse nanoparticles is the separation of nucleation and growth in time. This separation assumes that the nuclei form first, then grow, consuming the remaining precursor, as experimentally proven by Watzky et. al. (1997; 2008). This growth may nevertheless be different for different nuclei in the solution, because of fluctuations in concentration which is a consequence of the molecular character of matter. The Gaussian distribution (neither volumes nor areas follow this type of distribution) is a consequence of the kinetic mechanism of the growth of nanoparticles. In fact, the experimental proportionality observed between $\overline{d}_{TEM}$ and σ_r (i.e. α quasi-constant) are constraints that are also a consequence of the acting mechanism and fluctuations. Fluctuations are very important in chemical systems in which diffusion and chemical reactions are taken as the only significant molecular processes, because there exists a coupling between them which generates long-range correlations (Keizer, 1987). The relation of fluctuations with the mechanism is out of the scope of this work and will be discussed in future papers. As a consequence of what has been stated before, when it is said that the nanoparticles are near-monodisperse, the word "near" refers to a value of α conditioned by the synthesis method. In Finke's case, this value is ±15 %, while in the case of the modified polyol method used by us; it is of a ±26 %.

In order to have a quantitative idea about the way fluctuations affect specific area and diameters, the following hypothetical case has been discussed. The specific geometric area $\overline{A}$ depends on the two Gaussian parameters α and $\overline{d}$ (eq. (A.19)). Eq. (A.22) offers another expression for $\overline{A}$ which depends on the inverse of the cubic root of c_P^i and α. In our case, with $\alpha = (0.26 \pm 0.04)$, a (5.6±1.4) % decrease in the specific geometric area with respect to the value for a hypothetic monodisperse catalyst (i.e. a delta Dirac distribution, $\alpha = 0$) synthesized at same c_P^i, is apparent. Combining eqs. (A.19) and (A.22) we can obtain an expression for the

mean diameter in the Gaussian distribution, $\bar{d}(\alpha)$, with respect to the hypothetic diameter $\bar{d}(\alpha = 0)$, considering the same ρ_{np}, i.e. the same nucleation process:.

$$\frac{\bar{d}(\alpha)}{\bar{d}(\alpha = 0)} = \frac{1}{(1 + 3\alpha^2)^{1/3}} \tag{7}$$

In our case this produces a (6±0.6) % decrease in the mean diameter with respect to the monodisperse diameter. Then, the effect of fluctuations is small, but has a significant effect to be taken into account.

4. Conclusions

In summary, the modified polyol method (with PVP) has been used in order to synthesize highly dispersed Pt nanoparticles on carbon black. A new and simple statistical and geometrical treatment is used to explain experimental results. Analyzing experimental data obtained by XRD, TEM and CV for different variables of synthesis the following conclusions were reached:

- The sizes of the Pt nanoparticles in the catalysts depend mainly on c_P^i.

- In the polyol modified method the concentration of nanoparticles in the solution ρ_{np} after synthesis was the same, independent of c_P^i and not related to the Pt load in the support.

- A factor of efficiency of electrochemical area η_A was defined for the range of c_P^i in which ρ_{np} was constant. Its value in the linear zone was equal to 0.77±0.12. According to this efficiency there is a (23±4) % decrease in electrochemical area with respect to the predicted area.

- The mean value of α was equal to 0.26 ± 0.04 for the syntheses method used in this work.

5. Acknowledgments

This work was financially supported by: Unidad de Actividad Materiales del Centro Atómico Constituyentes de la Comisión Nacional de Energía Atómica (UAM-CAC-CNEA). The Comité

Ejecutivo de Desarrollo e Innovación Tecnológica (CEDIT) and Consejo Nacional de Investigaciones Científicas y Técnicas (CONICET)

The author would like to especially thank R.E. Gonnet for her remarks concerning several parts of this paper.

6. References

Adzic, R.R. et al., 2007. Platinum monolayer fuel cell electrocatalysts. Topics in Catalysis 46(3-4), 249–262.

Bagotsky, V.S., 2009. Problems and Solutions. third. John Wiley & Sons, Inc.

Bergamaski, K., Pinheiro, A.L.N., Teixeira-Neto, E. and Nart, F.C., 2006. Nanoparticle size effects on methanol electrochemical oxidation on carbon supported platinum catalysts. The Journal of Physical Chemistry B 110(39), 19271–19279.

Besson, C., Finney, E.E. and Finke, R.G., 2005. A mechanism for transition-metal nanoparticle self-assembly. Journal of the American Chemical Society 127(22), 8179–8184.

Bock, C., Paquet, C., Couillard, M., Botton, G.A. and MacDougall, B.R., 2004. Size-selected synthesis of PtRu nano-catalysts: reaction and size control mechanism. Journal of the American Chemical Society 126(25), 8028–8037.

Chen, M. and Xing, Y., 2005. Polymer-mediated synthesis of highly dispersed Pt nanoparticles on carbon black. Langmuir 21(20), 9334–9338.

Chu, Y.-Y., Wang, Z.-B., Gu, D.-M. and Yin, G.-P., 2010. Performance of Pt/C catalysts prepared by microwave-assisted polyol process for methanol electrooxidation. Journal of Power Sources 195(7), 1799–1804.

Esparbé, I., Brillas, E., Centellas, F., Garrido, J.A., Rodríguez, R.M., Arias, C. and Cabot, P.-L., 2009. Structure and electrocatalytic performance of carbon-supported platinum nanoparticles. Journal of Power Sources 190(2), 201–209.

Geniès, L., Faure, R. and Durand, R., 1998. Electrochemical reduction of oxygen on platinum nanoparticles in alkaline media. Electrochimica Acta 44(8–9), 1317–1327.

Keizer, J., 1987. Statistical Thermodynamics of Nonequilibrium Processes. Springer-Verlag, Inc.

Kim, J.W. et al., 2011. Size-controlled synthesis of Pt nanoparticles and their electrochemical activities toward oxygen reduction. International Journal of Hydrogen Energy 36(1), 706–712.

Kinoshita, K., 1990. Particle size effects for oxygen reduction on highly dispersed platinum in acid electrolytes. Journal of The Electrochemical Society 137(3), 845–848.

Leontyev, I.N., Belenov, S.V., Guterman, V.E., Shaganov, A.P. and Dkhil, B., 2011. Catalytic Activity of Carbon-Supported Pt Nanoelectrocatalysts . Why reducing the size of Pt nanoparticles is not always beneficial. Journal of Physical Chemistry C 115, 5429–5434.

Liu, H., Song, C., Zhang, L., Zhang, Jiujun, Wang, H. and Wilkinson, D.P., 2006. A review of anode catalysis in the direct methanol fuel cell. Journal of Power Sources 155(2), 95–110.

Maillard, F., 2002. Oxygen electroreduction on carbon-supported platinum catalysts. Particle-size effect on the tolerance to methanol competition. Electrochimica Acta 47(21), 3431–3440.

Nesselberger, M., Ashton, S., Meier, J.C., Katsounaros, I., Mayrhofer, K.J.J. and Arenz, M., 2011. The particle size effect on the oxygen reduction reaction activity of Pt catalysts: influence of electrolyte and relation to single crystal models. Journal of the American Chemical Society 133(43), 17428–33.

Nores-Pondal, F.J., Vilella, I.M.J., Troiani, H., Granada, M., de Miguel, S.R., Scelza, O. a. and Corti, H.R., 2009. Catalytic activity vs. size correlation in platinum catalysts of PEM fuel cells prepared on carbon black by different methods. International Journal of Hydrogen Energy 34(19), 8193–8203.

Oh, H., Oh, J., Hong, Y. and Kim, H., 2007. Investigation of carbon-supported Pt nanocatalyst preparation by the polyol process for fuel cell applications. Electrochimica Acta 52, 7278–7285.

Oh, H.-S., Oh, J.-G. and Kim, H., 2008. Modification of polyol process for synthesis of highly platinum loaded platinum–carbon catalysts for fuel cells. Journal of Power Sources 183(2), 600–603.

Perez, J., Gonzalez, E.R. and Ticianelli, E. a., 1998. Oxygen electrocatalysis on thin porous coating rotating platinum electrodes. Electrochimica Acta 44(8-9), 1329–1339.

Pozio, A., De Francesco, M., Cemmi, A., Cardellini, F. and Giorgi, L., 2002. Comparison of high surface Pt/C catalysts by cyclic voltammetry. Journal of Power Sources 105(1), 13–19.

Prabhuram, J., Wang, X., Hui, C.L. and Hsing, I.-M., 2003. Synthesis and Characterization of Surfactant-Stabilized Pt/C Nanocatalysts for Fuel Cell Applications. The Journal of Physical Chemistry B 107(40), 11057–11064.

Prabhuram, J., Zhao, T.S., Wong, C.W. and Guo, J.W., 2004. Synthesis and physical/electrochemical characterization of Pt/C nanocatalyst for polymer electrolyte fuel cells. Journal of Power Sources 134(1), 1–6.

Roucoux, A., Schulz, J. and Patin, H., 2002. Reduced transition metal colloids: a novel family of reusable catalysts? Chemical reviews 102(10), 3757–3778.

Senthil Kumar, S.M., Soler Herrero, J., Irusta, S. and Scott, K., 2010. The effect of pretreatment of Vulcan XC-72R carbon on morphology and electrochemical oxygen

reduction kinetics of supported Pd nano-particle in acidic electrolyte. Journal of Electroanalytical Chemistry 647(2), 211–221.

Shao, Minhua, Peles, A. and Shoemaker, K., 2011. Electrocatalysis on platinum nanoparticles: particle size effect on oxygen reduction reaction activity. Nano letters 11, 3714–3719.

Vengatesan, S. et al., 2008. High dispersion platinum catalyst using mesoporous carbon support for fuel cells. Electrochimica Acta 54(2), 856–861.

Watzky, M.A. and Finke, R.G., 1997. Transition metal nanocluster formation kinetic and mechanistic studies. A new mechanism when hydrogen Is the reductant: slow, Continuous Nucleation and Fast Autocatalytic Surface Growth. Journal of the American Chemical Society 119(43), 10382–10400.

Watzky, M.A., Finney, E.E. and Finke, R.G., 2008. Transition-metal nanocluster size vs formation time and the catalytically effective nucleus number: a mechanism-based treatment. Journal of the American Chemical Society 130(36), 11959–11969.

Yano, H., Kataoka, M., Yamashita, H., Uchida, H. and Watanabe, M., 2007. Oxygen reduction activity of carbon-supported Pt-M (M = V, Ni, Cr, Co, and Fe) alloys prepared by nanocapsule method. Langmuir 23(11), 6438–6445.

Zhang, J, Vukmirovic, M.B., Sasaki, K., Uribe, F. and Adzic, R.R., 2005. Platinum monolayer electrocatalysts for oxygen reduction: Effect of substrates, and long-term stability. Journal of the Serbian Chemical Society 70(3), 513–525.

Zhao, J., Jarvis, K., Ferreira, P. and Manthiram, A., 2011. Performance and stability of Pd–Pt–Ni nanoalloy electrocatalysts in proton exchange membrane fuel cells. Journal of Power Sources 196(10), 4515–4523.

Zhou, W., Zhou, Z., Song, S., Li, W., Sun, G., Tsiakaras, P. and Xin, Q., 2003. Pt based anode catalysts for direct ethanol fuel cells. Applied Catalysis B: Environmental 46(2), 273–285.

Appendix A

Relationship between ECSA and the inverse of the cubic root of initial concentration of precursor

The mathematical treatments of the appendix are not based on the mechanism itself, they are pure statistical and geometrical analyses based on some final results of the syntheses (spherical nanoparticles, Gaussian distribution of the diameters, etc.). Nevertheless, the validity of certain new restraints that are deduced between parameters (e.g. relations between ρ_{np}, σ_d with c_P^i), are a consequence of the nature of the mechanism itself.

Taking into account the experimental facts that the diameters of nanoparticles have a Gaussian distribution, the fraction of nanoparticles with radius r between r and r+dr is equal to:

$$\frac{dN_{np}(r)}{N_{np}^{T}} = \int_{r}^{r+dr} \frac{1}{\sigma_r \sqrt{2\pi}} \exp\left[-\frac{(r-\bar{r})^2}{2\,\sigma_r^{\,2}} \right] dr \tag{A.1}$$

The total volume differential $\mathrm{d}V^{T}(r)$ between r and r+dr can be obtained by multiplying the volume of each nanoparticle radius r by the number of nanoparticles having this radius, i.e. $\mathrm{d}N_{np}(r)$, then:

$$\mathrm{d}V^{T}(r) = V(r)\,\mathrm{d}N_{np}(r) = \frac{4\pi}{3}\, N_{np}^{T} \int_{r}^{r+\mathrm{d}r} r^3\, \frac{1}{\sigma_r \sqrt{2\pi}} \exp\left[-\frac{(r-\bar{r})^2}{2\,\sigma_r^{\,2}} \right] \mathrm{d}r \tag{A.2}$$

Integrating Eq. (A.2) between $-\infty$ and $+\infty$ we obtain the total volume equal to:

$$V^{T} = \frac{MW\, c_P^{i}\, V_r}{\rho_M} \tag{A.3}$$

Changing variables:

$$\mu = r - \bar{r};\ \ \mathrm{d}\mu = \mathrm{d}r \tag{A.4}$$

We obtain:

$$V^{T} = \frac{MW\, c_P^{i}\, V_r}{\rho_M} = \frac{4\pi}{3}\, N_{np}^{T} \int_{-\infty}^{+\infty} \frac{1}{\sigma_r \sqrt{2\pi}} (\mu + \bar{r})^3 \exp\left(-\frac{\mu^2}{2\sigma_r^{\,2}} \right) \mathrm{d}\mu \tag{A.5}$$

Considering relative standard deviation α defined as:

$$\alpha = \frac{\sigma_r}{\bar{r}} = \frac{\sigma_d}{\bar{d}} \ \text{ with } \ \alpha < 1 \tag{A.6}$$

When we consider that:

$$(\mu + \bar{r})^3 = \mu^3 + 3\mu^2\, \bar{r} + 3\mu\, \bar{r}^2 + \bar{r}^3 \tag{A.7}$$

Eq. (A.5) results to be the addition of four defined integrals, two of which equal zero (odd function), and two result equal to:

$$V^T = \frac{MW\, c_P^i\, V_r}{\rho_M} = \frac{4\pi}{3} N_{np}^T \frac{1}{\sigma_r \sqrt{2\pi}} \int_{-\infty}^{+\infty} (3\mu^2 \bar{r} + \bar{r}^3) \exp\left(-\frac{\mu^2}{2\sigma_r{}^2}\right) \mathrm{d}\mu \tag{A.8}$$

The integrals of μ^{2k} with $k = (0,1,2,...,+\infty)$ are the central moments of a symmetrically centred Gaussian distribution, which result to be different from zero and equal to:

$$\int_{-\infty}^{+\infty} \frac{1}{\sigma_r \sqrt{2\pi}} \mu^{2k} \exp\left(-\frac{\mu^2}{2\sigma_r{}^2}\right) \mathrm{d}\mu = \frac{2k!}{2^k\, k!} \sigma^{2k} \tag{A.9}$$

From eqs. (A.6), (A.8) and for $k = 0$ and 1 we finally obtain:

$$V^T = \frac{MW c_P^i\, V_r}{\rho_M} = \frac{4\pi}{3} N_{np}^T\, \bar{r}^3 + 4\pi N_{np}^T\, \bar{r}\, \sigma_r{}^2 = \frac{4\pi}{3} N_{np}^T (1+3\alpha^2)\, \bar{r}^3 \tag{A.10}$$

The relationship between V_m and c_P^i is obtained from this last equation:

$$V_m = \frac{4\pi}{3} \bar{r}^3 = \frac{V_r MW}{(1+3\alpha^2)\rho_M\, N_{np}^T} c_P^i = \frac{MW}{(1+3\alpha^2)\rho_M\, \rho_{np}} c_P^i \tag{A.11}$$

We will now calculate the value of the specific geometric area of the system, such value relates to the area experimentally calculated by CV (ECSA). The differential of total area $\mathrm{d}A^T(r)$ of nanoparticles with diameters between r and r+dr can be obtained by multiplying the area of each nanoparticle radius r by the number of nanoparticles with this radius, $\mathrm{d}N_{np}(r)$:

$$\mathrm{d}A^T(r) = A(r)\, \mathrm{d}N_{np}(r) = 4\pi\, N_{np}^T \int_r^{r+\mathrm{d}r} r^2 \frac{1}{\sigma_r \sqrt{2\pi}} \exp\left[-\frac{(r-\bar{r})^2}{2\,\sigma_r{}^2}\right] \mathrm{d}r \tag{A.12}$$

Changing variables,

$$\mu = r - \bar{r};\ \mathrm{d}\mu = \mathrm{d}r \tag{A.13}$$

and integrating Eq. (A.12) between $-\infty$ and $+\infty$ we reach:

$$A^T = 4\pi N_{np}^T \int_{-\infty}^{+\infty} \frac{1}{\sigma_r \sqrt{2\pi}} (\mu + \bar{r})^2 \exp\left(-\frac{\mu^2}{2\sigma_r{}^2}\right) \mathrm{d}\mu \tag{A.14}$$

Opening the expression:

$$(\mu+\bar{r})^2 = \mu^2 + 2\mu\,\bar{r} + \bar{r}^2 \tag{A.15}$$

Eq. (A.14) results to be the addition of three defined integrals one of which equals zero and the two other integrals equal to:

$$A^T = 4\pi N_{np}^T \int_{-\infty}^{+\infty} \frac{1}{\sigma_r \sqrt{2\pi}} (\mu^2 + \bar{r}^2) \exp\left(-\frac{\mu^2}{2\sigma_r{}^2}\right) d\mu \tag{A.16}$$

From eqs. (A.6) and (A.9) with $k = 0$ and 1 and the last one, we see that

$$A^T = 4\pi N_{np}^T \bar{r}^2 + 4\pi N_{np}^T \sigma_r{}^2 = 4\pi N_{np}^T (1+\alpha^2)\bar{r}^2 \tag{A.17}$$

If we divide this area by the total metal mass m_T using eq. (A.10) and metal density:

$$m_T = \rho_M V^T = \rho_M \frac{4\pi}{3} N_{np}^T (1+3\alpha^2) \bar{r}^3 \tag{A.18}$$

The specific area can be written as:

$$\overline{A} = \frac{3}{\rho_M} \frac{(1+\alpha^2)}{(1+3\alpha^2)} \frac{1}{\bar{r}} = \frac{6}{\rho_M} \frac{(1+\alpha^2)}{(1+3\alpha^2)} \frac{1}{\bar{d}} \tag{A.19}$$

Where the specific area is proportional to the inverse of r or $\bar{d}$.

On the other hand, replacing the value for r obtained from Eq. (A.11) we have:

$$A^T = 4\pi N_{np}^T (1+\alpha^2) \left(\frac{3MW\, c_P^i}{4\pi(1+3\alpha^2)\rho_M \rho_{np}}\right)^{2/3} \tag{A.20}$$

If we divide this area by the total mass m_T calculated now as:

$$m_T = MW\, c_P^i V_r \tag{A.21}$$

we obtain another expression for the specific geometric area $\overline{A}$, which depends on c_P^i, equal to:

$$\overline{A} = \frac{(1+\alpha^2)}{(1+3\alpha^2)^{2/3}} \left(\frac{36\,\pi\,\rho_{np}}{MW\,\rho_M^2}\right)^{-1/3} \frac{1}{c_P^{i\,1/3}} = F(\alpha) \left(\frac{36\,\pi\,\rho_{np}}{MW\,\rho_M^2}\right)^{-1/3} \frac{1}{c_P^{i\,1/3}} \tag{A.22}$$

We must also consider that the specific area measured electrochemically (ECSA) is equal to this specific area $\overline{A}$ multiplied by a factor η_A which ranges between 0 and 1 and are the

quotients between the effective area calculated from the hydrogen desorption and the geometrical area, this is:

$$ECSA = \eta_A F(\alpha)\left(\frac{36\,\pi\,\rho_{np}}{MW\,\rho_M^2}\right)^{1/3}\frac{1}{c_P^{i\,1/3}} = \eta_A\,\frac{(1+\alpha^2)}{(1+3\alpha^2)^{2/3}}\left(\frac{36\,\pi\,\rho_{np}}{MW\,\rho_M^2}\right)^{1/3}\frac{1}{c_P^{i\,1/3}} \qquad (A.23)$$

This equation shows that when there is a Gaussian distribution for the radii of nanoparticles, having a standard deviation σ_r, the electrochemical specific area ECSA depends on the inverse of the cubic root of c_P^i. The slope of the plot of this equation depends on the relative standard deviation through function $F(\alpha)$.

Captions

Figure 1. TEM and histograms of catalysts synthesized using initial concentrations of precursor (a) 12 mM, (b) 4 mM and (c) 2 mM.

Figure 2. Diffractograms of catalysts synthesized with: a) fixed c_P^i of 2 mM and Pt load 10 to 40 *wt.%,* b) different c_P^i values between 0.25 and 12 mM.

Figure 3. Relationship between diameters of nanoparticles calculated with XRD and TEM. Slope (0.80±0.02), intercept equal to (-0.15±0.08) nm. Correlation factor 0.992.

Figure 4. V_m vs. c_P^i. *Slope 1* = $(1.28 \pm 0.07)\,10^{-14}$ $cm^6\,M^{-1}$, intercept equal to (- 6.2±3.6) nm^3. Correlation factor: 0.986.

Figure 5. Voltammograms for catalysts synthesized with a) fixed c_P^i of 2 mM and Pt load 10 to 40 *wt.%*, b) different c_P^i (0.25 to 12 mM).

Figure 6. ECSA vs. c_M. *Slope 2* = $(81.3 \pm 2.9)\,m^2\,g^{-1}\,mM^{1/3}$, intercept equal to (0.4±2.5) $m^2\,g^{-1}$. Correlation factor 0.998.

Table I. Synthesis of catalysts carried out in the same initial concentration of the precursor (2mM), carbon changing to get the corresponding wt.% and PVP/Pt 0.1. Concentration of Pt in

Vulcan (wt.%) evaluated after synthesis by analytical methods, ECSA calculated by CV, nanoparticle diameters evaluated by XRD and TEM.

Table II. Catalyst synthesis performed with different initial concentrations of the precursor. Concentration of Pt in Vulcan (wt.%) evaluated after synthesis by analytical methods, ECSA calculated by CV, nanoparticle diameters evaluated by XRD and TEM.

Table 1

wt.% Nominal	*wt.%* measured	*ECSA* (m^2g^{-1})	$\bar{d}_{XRD}$ (nm)	$\bar{d}_{TEM} \pm \sigma_d$ (nm)	α
10	11.3	66±3	2.0	2.86 ± 0.66	0.23
20	19.7	63±4	2.3	2.80 ± 0.78	0.28
30	29.3	63±3	2.3	3.00 ± 0.66	0.22
40	39.6	63±1	2.8	3.60 ± 0.76	0.21

Table 2

c_M (mM)	*wt.%* measured	ECSA (m^2g^{-1})	$\bar{d}_{XRD}$ (nm)	$\bar{d}_{TEM} \pm \sigma_d$ (nm)	α
0.25	11.3	67	1.6	2.20 ± 0.66	0.301
0.5	8.7	100	1.6	2.40 ± 0.66	0.275
1	10.3	85	1.9	2.20 ± 0.46	0.210
2	11.3	66	2.0	2.86 ± 0.68	0.239
4	11.0	50	2.9	3.86 ± 0.95	0.246
8	10.2	33	4.3	5.60 ± 1.52	0.273
12	10.0	24	5.3	6.20 ± 2.05	0.330

Highlights

- The sizes of the Pt nanoparticles in the catalysts mainly depend on precursor initial concentration.
- The concentration of nanoparticles is fixed and independent of the precursor initial concentration.
- Between XRD and TEM a good correlation of crystallite sizes and mean diameter is observed.

Fig. 1

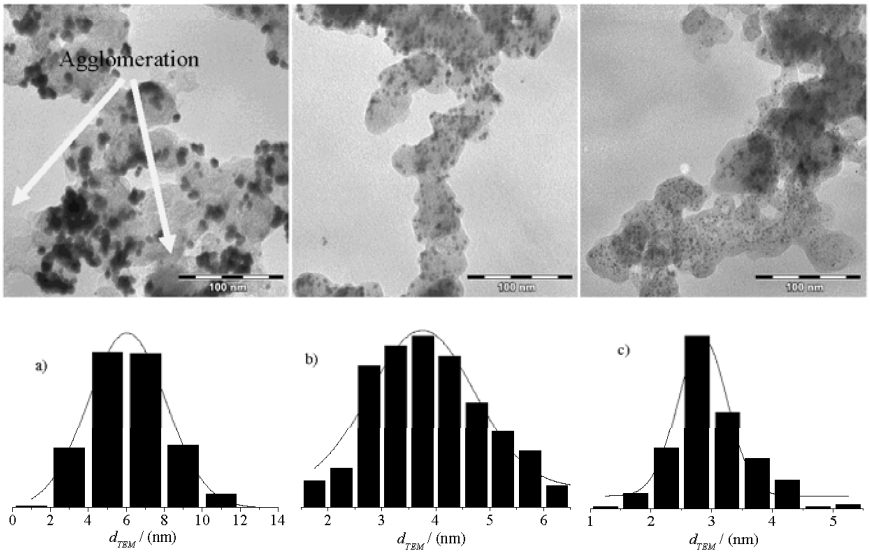

Fig. 2

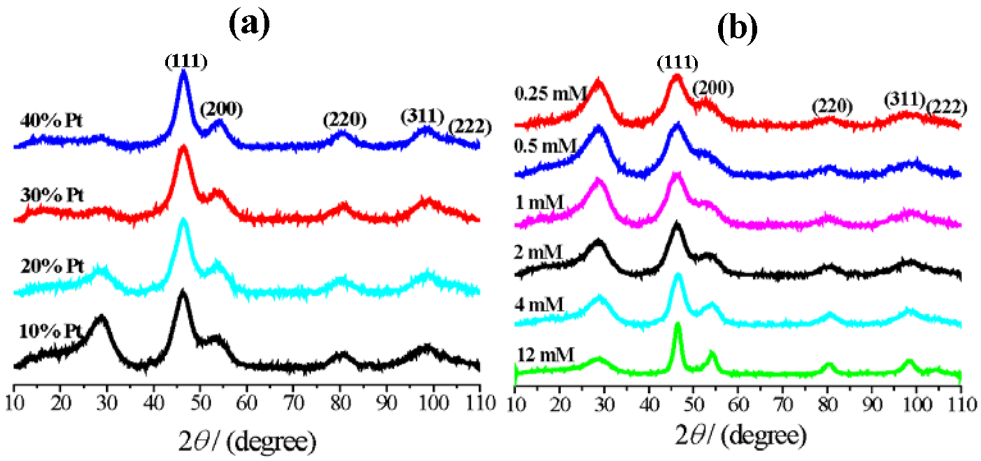

Fig. 3

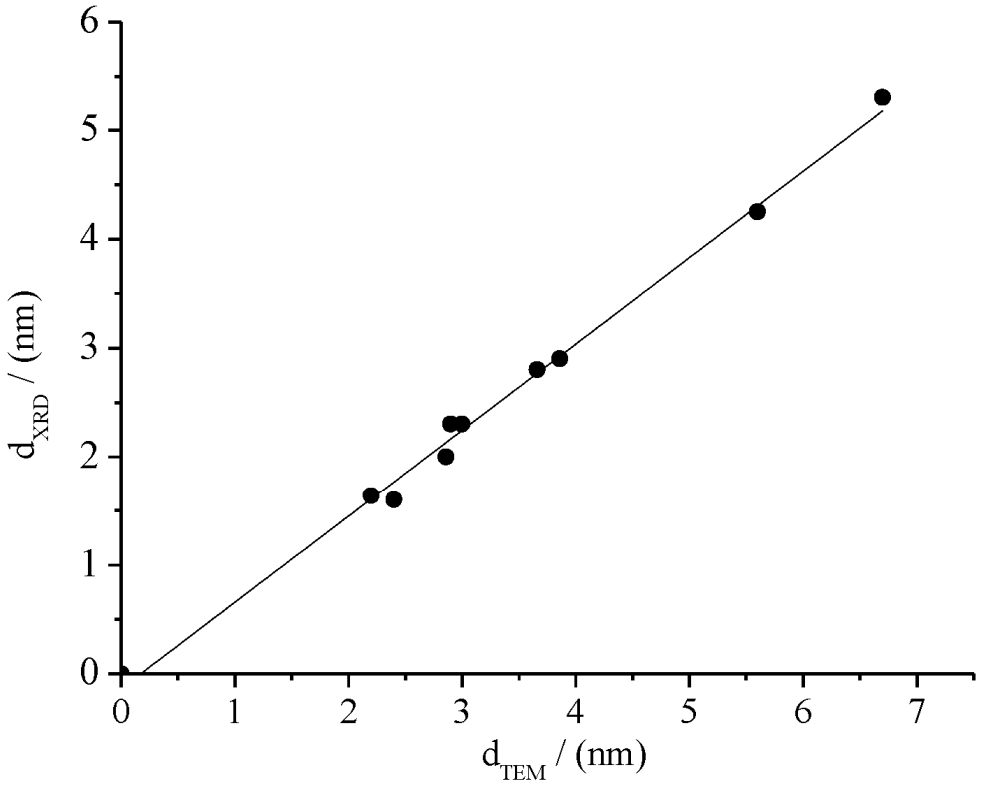

Fig. 4

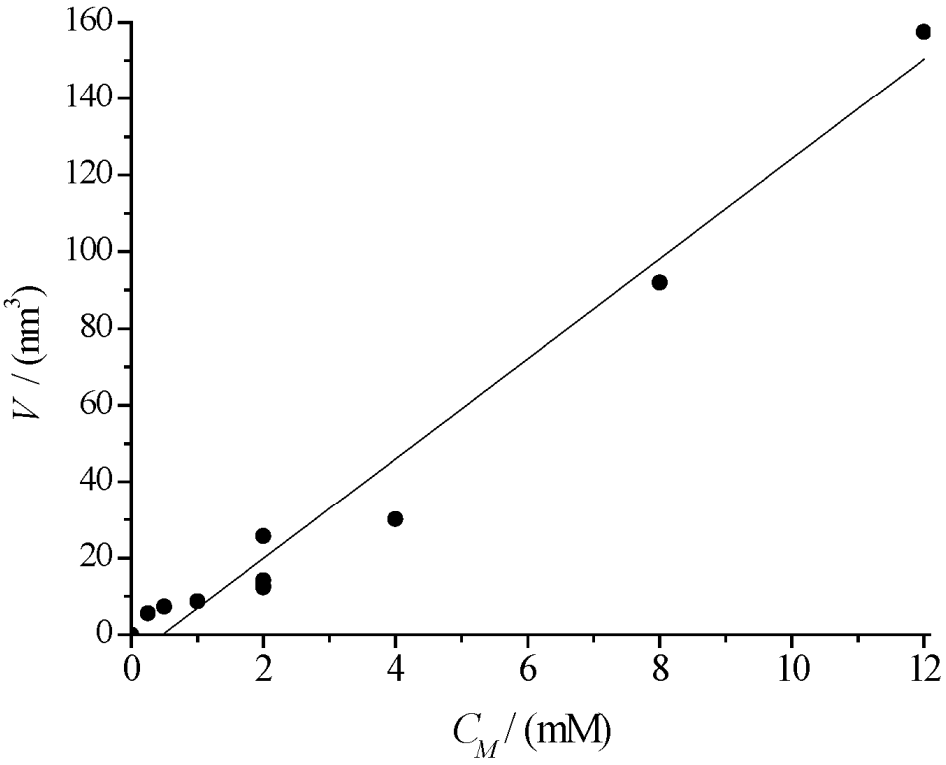

Fig. 5

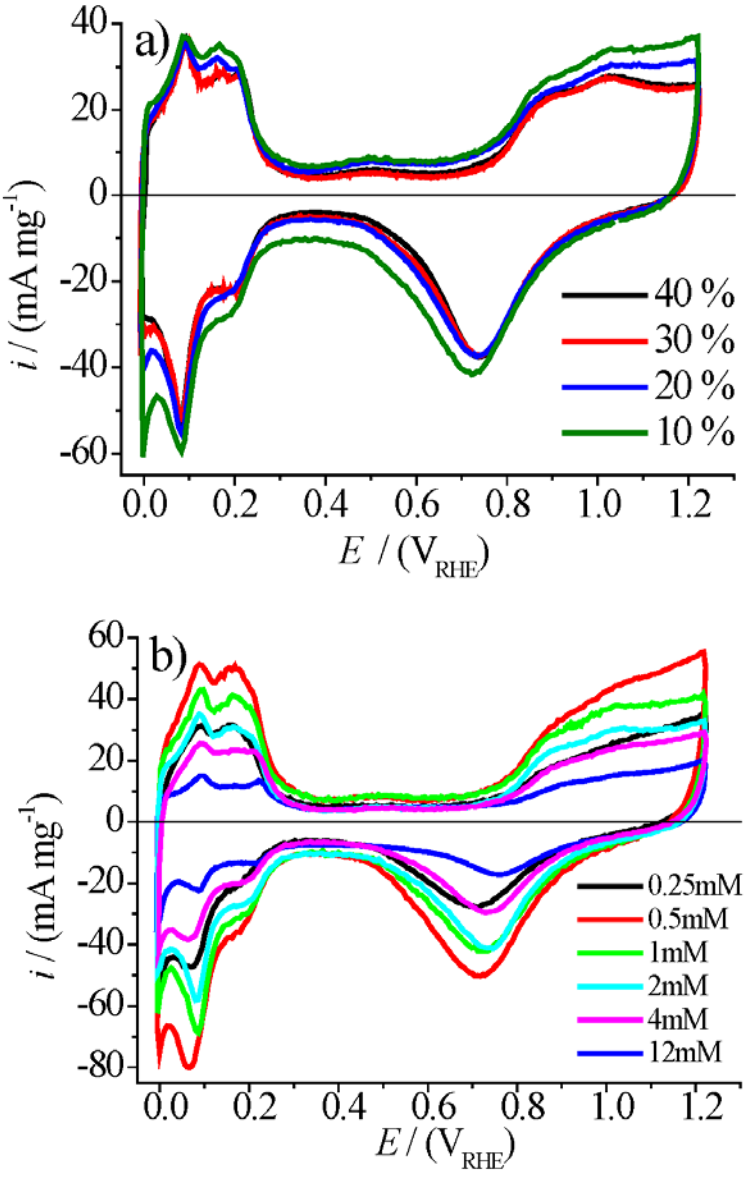

Fig. 6